Scanning Microscopy

Volume 2 | Number 2 Article 3

2-3-1988

The Depth Resolution of Secondary Ion Mass Spectrometers: A Critical Evaluation

D. S. McPhail
University of Warwick

E. A. Clark
University of Warwick

J. B. Clegg
Philips Research Laboratories

M. G. Dowsett
University of Warwick

J. P. Gold
Imperial College

See next page for additional authors

The Depth Resolution of Secondary Ion Mass Spectrometers: A Critical Evaluation

Authors

D. S. McPhail, E. A. Clark, J. B. Clegg, M. G. Dowsett, J. P. Gold, G. D. T. Spiller, and D. Sykes

Scanning Microscopy, Vol. 2, No. 2, 1988 (Pages 639-652) 0891-7035/88$3.00+.00
Scanning Microscopy International, Chicago (AMF O'Hare), IL 60666 USA

THE DEPTH RESOLUTION OF SECONDARY ION MASS SPECTROMETERS: A CRITICAL EVALUATION

D.S. McPhail[1] *, E.A. Clark[1], J.B. Clegg[2], M.G. Dowsett[1], J.P. Gold[3], G.D.T. Spiller[4] and D. Sykes[5].

* 1. Dept. of Physics, University of Warwick, Coventry CV47AL, England, UK.
2. Philips Research Laboratories, Redhill, Surrey, England.
3. Surface Analysis Technology, Imperial College, London SW7, England.
4. British Telecom Research Laboratories, Martlesham Heath, Ipswich, England
5. Loughborough Consultants Ltd., Loughborough University, Loughborough, England

(Received for publication April 01, 1987, and in revised form February 03, 1988)

Abstract

The ability of five Secondary Ion Mass Spectrometry (SIMS) instruments to resolve thin layer and modulated dopant structures by depth profiling has been assessed. Three magnetic sector instruments (two Cameca IMS 3f's and one 4f), which use optical gating and a high extraction field, were used, together with two different quadrupole based instruments (EVA 2000 and Atomika), which use electronic gating and a low extraction field. The test structure, a thirty-one peak boron-in-silicon modulating dopant structure, was grown by Molecular Beam Epitaxy (MBE).

In all the depth profiles the near surface peaks appeared narrow and asymmetric, being broadened only by fundamental processes (e.g., atomic mixing and recoil implantation). As the profiles proceeded, however, further broadening was observed. This phenomena varied markedly both from one instrument to another and from one experiment to another on the same instrument. In some cases the loss of depth resolution with depth was manifested by broadening mainly in the leading edge, in others the trailing edge, of successive boron peaks. The 'order of merit' of the instruments thus depended on the parameter used to define depth resolution.

The loss of peak (depth) resolution with depth was due to variations in primary ion beam density across the gated area of the crater, which led to uneven etching. The changes in peak shape with depth can be explained by a numerical model of the etching process. These observations dictate that the depth resolution of a SIMS instrument should not be measured in terms of a single interface width, such as the leading or trailing edge.

KEY WORDS: Secondary Ion Mass Spectrometry, Low Dimensional Structures, Silicon Molecular Beam Epitaxy, Depth Resolution, Topography, Diffusion, Ion Beam Lithography, Bevelling, Etching, Imaging.

*Address for correspondence:
Department of Physics, Warwick University,
Coventry CV4 7AL, England, UK.
Phone No. (UK) 0203 523871.

Introduction

As the performance characteristics (lateral resolution, depth resolution, sensitivity) of Secondary Ion Mass Spectrometry (SIMS) are continuously improved and the various problems associated with the technique are better understood the analyst can tackle with confidence an increasing number of materials problems (Honig 1986). Unfortunately analysis of some of the most technologically interesting materials require lateral and depth resolutions close to or beyond the performance limitations of the technique. Consider, for example, the range of novel materials termed low dimensional structures (LDS). Low dimensional structures are solids, often semi-conductors, in which the scale of the structure is very small in one or more directions thus leading to the quantisation of electronic states in the constrained directions and to the possibility of novel electronic devices (e.g., quantum well lasers). Layer widths can be nanometres or less and the interfaces between layers can be atomically abrupt. Analysis of such sharp interfaces using SIMS depth profiling is hindered by the lateral and vertical mixing processes inherent in sputtering. Furthermore SIMS is a destructive analytical technique and attempts to reduce the analytical area or the depth increment per data point will lead to a loss of sensitivity. Much effort is being expended to improve the lateral resolution, the depth resolution and the sensitivity of the technique and to develop novel analysis strategies.

The current state-of-the-art lateral resolution is due to Levi-Setti et al (1985) who has recently reported a lateral resolution from his 55keV gallium liquid metal ion source (LMIS) of 20nm. A number of commercial guns that form the basis of SIMS imaging instruments now routinely achieve a figure only a decade worse. This figure (20nm) is close to the lateral width of the collision cascade for heavy ions; further improvements in lateral resolution will require a technology that allows use of lighter species and / or lower energies.

The ultimate limit to the depth resolution in SIMS depth profiling arises from the fact that a finite volume of material must be consumed per data point. As the depth increment per data point,

dz, is decreased so also is the analytical volume and thus the count-rate (the analytical area, A, is limited in present day instruments to a circle or square a few thousand microns across). In general the relationship between the micro-volume sputtered per data point, the number of ions detected, N, and the detection limit, C, is given by (Williams 1985);

$$C = N / [(aT)Adz] \qquad (1)$$

where the product of the ionisation coefficient, a, and the instrumental transmission, T, is termed the useful yield. It is clear that to attain high resolution in one or more directions one has to sacrifice sensitivity. This consideration has led researchers to consider methods of increasing the ionisation coefficient a (which is usually less than 1%), by post-ionisation of the neutral secondaries. Lasers, electrical discharges, plasmas and thermal excitation are all being investigated at present (e.g. Gruen et al, 1987).

These calculations suggest that one could achieve monolayer depth resolution in SIMS depth profiling, albeit with poor sensitivity, by sputtering at a sufficiently low rate. However, the physics of the sputtering process itself precludes such a possibility. Sputtering involves the transfer of energy from the primary ion beam to the target atoms and leads to a collision cascade in the solid. The cascade mixing depth is similar to the range of the primary ions (Magee et al, 1982). There is, therefore, a redistribution of target atoms in the solid prior to sputtering and the surface layers from which the secondary ions are originating have lost their original chemical identity. It is this redistribution of dopant atoms prior to sputtering that, in practise, defines the ultimate achievable depth resolution once all instrumental and sample related problems have been eliminated. Typically fundamental effects (atomic mixing, recoil implantation, radiation enhanced diffusion, segregation) will broaden out an atomically abrupt planar marker layer over a depth of ten nanometres or more and will redistribute atoms laterally by several tens of nanometres (see above). These beam induced broadening effects can be minimised by appropriate choice of experimental conditions (Wittmaack and Wach 1981) often by lowering the probe energy, but can never be removed entirely. In any case, lowering the probe energy leads to a loss in primary beam current, which can make focussing more difficult, may increase differential sputtering and decrease the sputtering yield somewhat. It seems inevitable, therefore, that deconvolution techniques will play an increasing role in the SIMS analyses of very thin layer structures. King and Tsong (1985), for example, recently reported on a method of deconvoluting the broadening and shifting of peaks in SIMS depth profiles of buried Ti and Mo markers in silicon.

Fundamental effects usually lead to a broadening that is independent of the depth of the marker layer beneath the surface, provided only the depth exceeds the near-surface pre-equilibrium region of the profile. Surface microtopography, which is only observed with certain primary ion beam - matrix combinations, is an exception to this rule. For example sputtering of gallium arsenide with an oxygen primary ion beam leads to cone formation (Gavrilovic 1986), the cones get taller and the depth resolution worse as the profile proceeds. In general, however, it is instrumental problems that lead to a deterioration in depth resolution with depth. Werner (1982) has reported the results of several measurements on the depth resolution, dz, as a function of depth, z, defining the depth resolution as 'the depth which must be sputtered away, such that the signal from a step-function profile, assumed to follow an error function, drops from 84% to 16% of its maximum value' In all cases Werner found that the depth resolution deteriorated as the the profile proceeded. He argued that the data sets could be fitted to a curve of the form;

$$dz(nm) = a + Bz^{l} \qquad (2)$$

where l was close to unity, $1.9nm < a < 14.2nm$ and $0.001 < B < 0.047$. The B term usually arises from instrumental problems such as non-uniform etching due to non-linear scanning of the primary ion beam or from materials problems such as the presence of particulates on the initial surface or occlusions within the material. It occasionally contains a component due to the development of microtopography. Magee et al (1982) used a similar definition of the depth resolution for assessment of his instrument at RCA, He analysed an InGaAs / GaAs sample and monitored the indium signal as the interface was traversed. He reported a depth resolution of 5.5nm at $\sim 0.135\mu m$. It will be shown that characterization of the depth resolution of a SIMS instrument in this way is unsatisfactory. It may mask serious instrumental problems and give the analyst a false confidence in his instrument. It will be shown that measurements on both an up-slope and a down-slope are necessary. A better test sample for Magee's work would have been a GaAs/InGaAs/GaAs sample. Measurements could then have been made both on the rising indium signal at the first interface and the falling indium signal at the second interface giving a more complete picture, as in Magee et al (1978) with Ta_2O_5 films.

The depth resolutions Werner and Magee reported are often satisfactory for the SIMS depth profiling of dopant distributions produced by ion implantation or diffusion followed by annealing (one of the main tasks of many instruments over the last two decades) but are inadequate for many of the novel semi-conducting materials which will form the basis of devices in the next few decades, for example periodic dopant structures, superlattices and low dimensional structures. These materials often require nanometre resolution or less. It is clear that SIMS depth profiling must undergo considerable improvements both in terms of instrumentation, experimental procedure and theoretical modelling of the mixing processes if it is going to be a useful analysis technique for these materials. One important task, therefore, is to measure the depth resolution - depth characteristic, using a suitable test structure, to discover which of the SIMS instruments currently available is best suited to the analysis of such materials, and to discover the optimum experimental conditions for this

application. Such studies may then indicate neccessary improvements both to instruments and experimental procedures.

Recently we (McPhail et al, 1986) reported the result of SIMS depth profiling of a boron-in-silicon modulated dopant structure, grown by silicon Molecular Beam Epitaxy (MBE), containing thirty-one dopant 'spikes' $\sim$ 50nm apart. The boron rich layers were believed to be less than 10nm thick. This is clearly a demanding structure to analyse and as such is suitable for evaluating instrumental problems associated with the primary beam optics (non-uniform scanning, variations in beam current) and errors in the depth calibration procedures employed in different laboratories. Such information is transferable to other dopant-matrix combinations.

In the series of experiments reported here, we first conducted thermal cycling / SIMS depth profiling tests to check whether diffusion could have broadened the dopant peaks during the MBE growth. The sample was then analysed on five different instruments using a primary beam energy close to 4keV. One laboratory (A) also investigated the variation in the shape of the near-surface peaks as a function of primary beam energy.

Experimental

MBE growth of the test structure.

The silicon epilayer was grown in our V80 silicon MBE kit (VG Semicon). This instrument includes a silicon cell and four doping cells (boron, phosphorus, arsenic and antimony) (Kubiak et al 1985). The silicon was deposited on a 7.5cm diameter silicon substrate (<100> n^- 0.8 - 1.2 ohm cm^{-1}). The substrate was held at 750 $\pm$ 30 ^oC during the growth, which lasted 70 minutes, and boron-rich layers were produced by co-evaporation, manually ramping the output from the boron cell power supply up and down thirty times. (This operation can lead to imprecise doping and we now use a computer controlled power supply and shuttering). The mark to space ratio (boron cell on/off) was 1 to 3. It should be noted that variations in the substrate temperature across the wafer can be 30^oC and that variations in the silicon and boron flux across the solid angle defined by the source-wafer geometry can be several percent. This has implications for the SIMS analysis of samples taken from different parts of the wafer.

Thermal cycling of the grown wafer.

Four 5mm square samples were sectioned from the wafer and placed in silica ampoules, which were then evacuated and sealed. Three of the ampoules were introduced into the hot-zone of a furnace, which was at the original sample growth temperature, and left there for 2 minutes (the time the sample requires to warm up and cool down), 60 minutes and 240 minutes, respectively. The fourth was a control. The ampoules were carefully fractured and the samples removed for SIMS depth profiling of the near-surface peaks (pk2 and pk3).

SIMS analyses of the test structure.

5mm squares were sectioned from the wafer and distributed to five SIMS laboratories throughout England. The instruments/laboratories involved were designated A to E. The analysts were invited to depth profile the samples for the major boron isotope (^{11}B) and to select the optimal

Table 1

Instrumental designations and experimental conditions used for the SIMS analyses of the test structure

Lab/ Inst.	Primary Beam		Secondary Ion Collection			Profile rate				
	E kV	I μA	Crater μm	gate μm	Vext kV	Depth μm	Time min	frames	dz nm	SR nm/sec
A1	3.5	0.5	400	8 (O)	4.5	1.770	87.4	499	3.55	0.338
A2	3.5	0.5	400	60 (O)	4.5	1.638	89.0	487	3.36	0.307
B	5.5	0.443	500	62 (O)	4.5	1.646	89.2	487	3.38	0.308
C	4.0	0.3	500	35 (O)	4.5	1.901	100.0	2000	0.95	0.316
D1	4.0	0.083	400	175 (E)	0.2	1.670	651.3	1303	1.28	0.043
D2	4.0	0.083	400	175 (E)	0.2	0.768	224.7	450	1.70	0.057
E	4.0	0.3	600	160 (E)	0.2	0.777	240.0	377	2.06	0.052

A1 & A2 = Cameca IMS3F; B = Cameca IMS 4F; C = Cameca IMS 3F; D1 & D2 = EVA 2000; E = Atomika DIDA ion microprobe. The primary ion species was O_2^+ (32 a.m.u.) in all cases. Crater = length of square crater side. Gate = linear dimension of the area in the centre of the crater from which secondaries are collected, either optically (O) with a circular gate or electronically (E) with a square gate. In the latter case one must take account of the finite beam width. Vext = secondary ion extraction voltage. Depth = total crater depth. Time = duration of experiment. Frame = number of times the boron channel was selected during the experiment. dZ = the depth increment between boron data points. SR = the sputter rate in the experiment.

experimental conditions for the analysis. That is, to choose conditions of beam energy, beam current, gated area and data collection period/frame time that produced a reasonably high count-rate and rapid profiling speed (thus minimising statistical fluctuations and instrumental drift) whilst retaining an acceptable data density. In particular the analysts were asked to work at a primary beam energy close to 4keV ($^{16}O_2^+$) and to gate the secondaries from a small area of the crater. Details of the instruments and of the analysis conditions used are given in (Table 1). Two laboratories (A and D) repeated the analysis having modified their experimental conditions, thus yielding seven analyses in all.

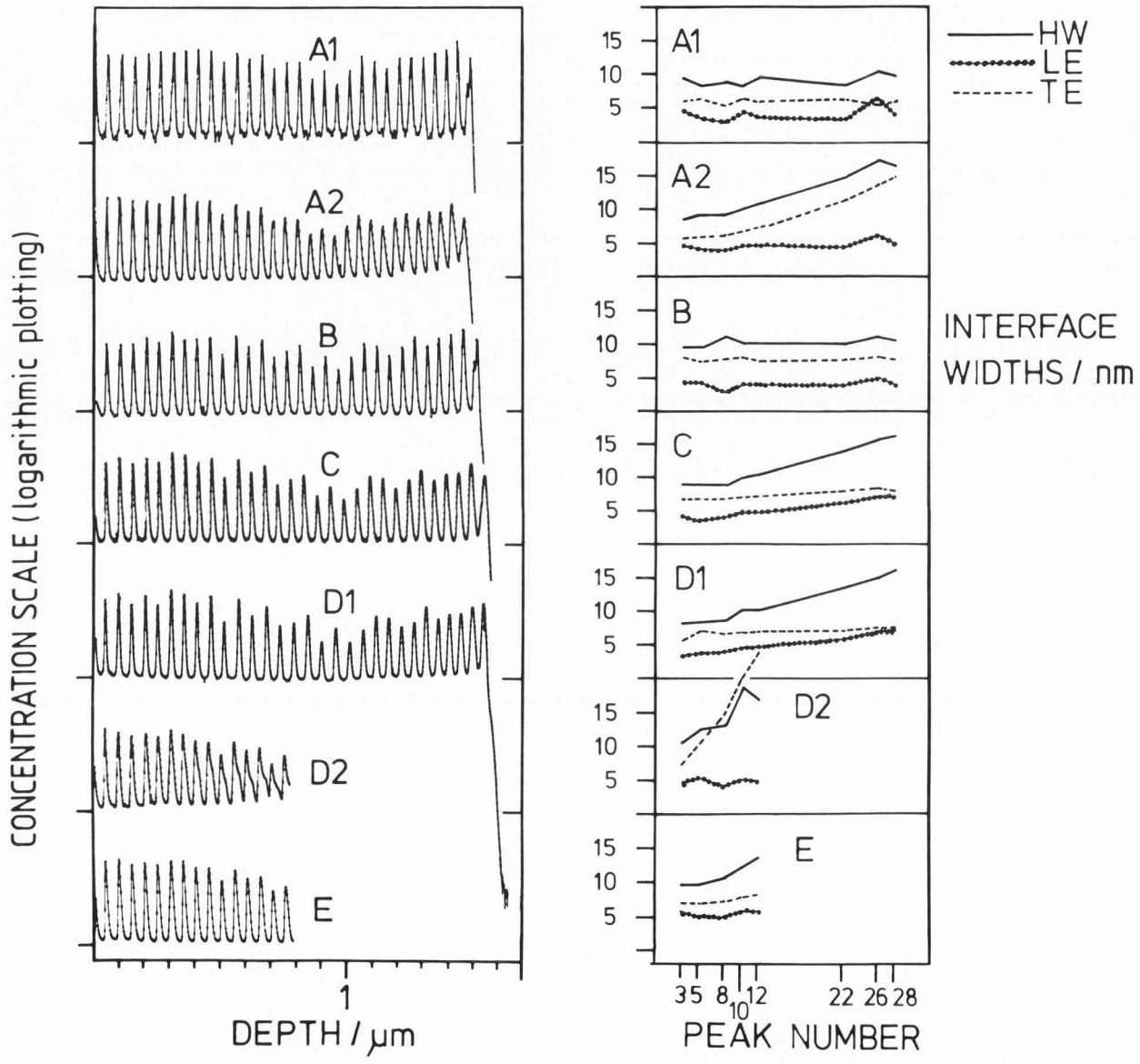

Figure 1.

The combined results of seven depth profiles of the MBE boron-in-silicon test sample. Five different instruments (A, B, C, D, E) were used. The experimental conditions are given in Table 1. We also plot the peak interface widths as a function of sputtered depth in this Figure.

Results and Discussion

Thermal cycling experiments on the test structure

The thermally cycled samples were depth profiled on our SIMS instrument, EVA 2000 (Dowsett and Parker 1983). We wished to determine whether the peaks would broaden if heated to the growth temperature. Only the near surface peaks were depth profiled to minimise the effects of uneven etching, which would confuse the issue. The observed changes in the interface widths were less than the experimental uncertainties introduced by depth calibration and instrumental drift (5%). We were thus assured that diffusion was unlikely to have significantly altered the peak interface widths during the MBE growth. This is important as diffusion during growth would affect the deepest peaks the most so its effects could very easily be confused with the effects of uneven etching during analysis, for example by SIMS (McPhail et al, 1987) electrochemical C-V profiling or Auger depth profiling.

SIMS depth profiles on the test structure

The results of SIMS depth profiling of the sample by five different instruments, using the conditions given in Table 1, are shown in Figure 1. The analyst from laboratory A (Cameca IMS 3F) conducted two consecutive experiments changing one parameter, the gated area, from 8μm diameter to 60μm diameter between experiments A1 and A2. The two profiles from instrument D (EVA 2000) represent results on different days but with nominally identical experimental conditions. The concentration scales of all profiles have been forced equal (the inter-peak concentration set at 10^{19} atoms cm^{-3}) but the depth scales left as measured. There are significant differences between the profiles, although the trends in peak size are consistent. The peaks are taller and sharper in experiments A1 and B, and show no tendency to broaden with depth. There is significant broadening in all other profiles. Results A1 and B confirm that diffusion during growth was not significant. The positions of peak 31 in experiments A1, A2, B, C and D1 were 1.467μm, 1.490μm, 1.511μm, 1.545μm, and 1.535μm, repectively, yielding a mean of 1.510μm and a standard deviation of 0.03μm (1.6%). Given that crater depth measurements (Dektak - instrument C , Talystep - instruments A,B,D,E) are only considered accurate to a few percent this is a fair agreement. The discrepancy is, however, sufficient to introduce a difference, between A1 and D1 of more than one peak spacing, which could represent a real difference in epilayer thickness across the wafer. The depths of craters A1 and D1 were remeasured on the same Talystep at the same time and the differences confirmed. It would perhaps be more correct to draw the profiles with the deepest peaks (e.g., the substrate positions) coincident and the surfaces misaligned.

As the trends in peak height are reproducible between experiments, it follows that successive boron-rich layers do not contain either the same peak concentration or the same amount of dopant, due to problems during growth. The areas under the peaks were evaluated and peaks 3, 5, 8, 10, 12, 22, 26 and 28 found to be similar in these repects (Figure 2). These peaks only were used for further comparisons. (Note: the surface level is counted as peak 1, the first complete peak, as peak 2)

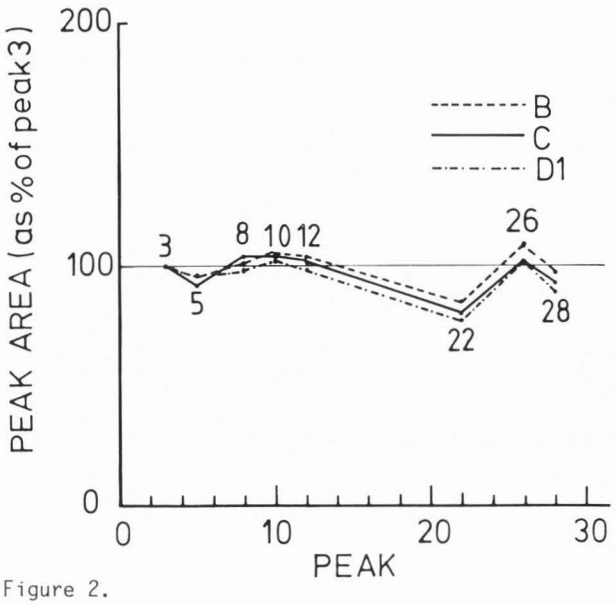

Figure 2.

The amount of dopant contained in layers 3, 5, 8, 10, 12, 22, 26 and 28 as a percentage of that in layer 3. These are the best layers (peaks) for inter-comparison.

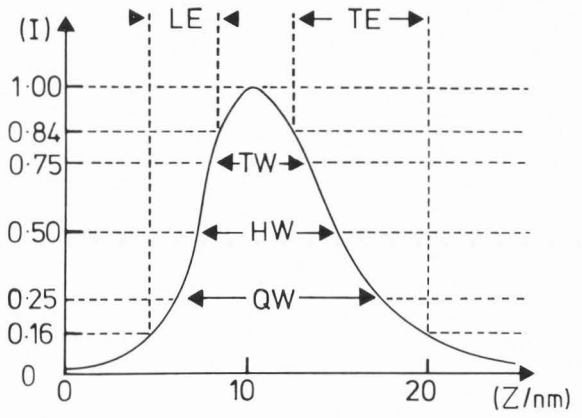

Figure 3.

The definitions used for calculating the interface widths. The decay lengths are defined as d(ln I)/dz where I is the secondary ion intensity and z the depth.

The manner and the extent of the peak broadening clearly varied from experiment to experiment and this was quantified by measuring the peak widths in various ways, Figure 3. The full-width-at-three-quarters-maximum (TW), full-width-at-half-maximum (HW), the full-width-at-one-quarter maximum (QW) and the interface widths from 16% to 84% of peak height

were all measured for the reference peaks (3, 5, 8, 10, 12, 22, 26, 28). When plotted on a logarithmic scale the peak up-slope and down-slope were often found to be close to linear and, where appropriate, the up-slope (LU) and down slope (LD) (decay lengths) were calculated. The inter-peak background of 10^{19} cm^{-3} was subtracted before measuring LE and TE. The HW and the interface widths (LE, TE) are plotted as a function of peak number / depth in Figure 1. The large differences in instrumental performance are apparent. In experiments A1 and B there is no significant degradation in depth resolution with depth between peak 3 and peak 28 (< 1nm), a depth interval of 1,250nm, whereas in all other experiments there is.

The changes in depth resolution with depth between peak 3 and peaks 26 / 28 (average of two) are shown in Figure 4. The percentage changes (dz/z).100 are equivalent to the B definition used by Werner (when expressed as a percentage). The performance of the Camecas in experiments A1 and B are indeed excellent, with a degradation in the peak widths (HW) of less than 0.1%. This is particularly impressive in the case of experiment B, where a relatively large gated area was used (62μm diameter circle compared with A1, where it was 8μm). The Cameca in experiments A2 (gate = 60μm diameter circle) and C (gate = 35μm circle) and EVA 2000 in experiment D1 (electronic gate = 175μm square) did less well, the loss of depth resolution (HW) being between 0.6% and 0.7% (7.2nm to 8.7nm). The values in Figure 4 for experiments E and D2 had to be extrapolated (EVA 2000, gate = 175μm square: Atomika, gate = 160μm square). These two experiments (D2, E) were worse still, particularly D2 (EVA 2000), where there was severe loss of depth resolution with depth. That experiment had to be terminated at peak 16, for the trailing edge of the peak was interfering with the leading edge of the next.

It is most important to note, furthermore, that the 'order of merit' of the experiments (loss of depth resolution with depth) depends upon the the choice of interface width used to measure it (e.g. LE, TE, HW). For in experiments C and D1 most of the change in peak shape was in the leading edge whereas in experiments A2, E and D2 most of the change in peak shape was in the trailing edge. Had the depth resolution of instrument D in experiment D2 been measured in terms of the leading edge interface width it would appear that the instrument was working well (B = 0.12%), whereas measurement on the trailing edge would reveal the gross problem in fact present (B = 3.8%). It is also important to note that as the peaks are progressively broadened the peak height decreases (although the integrated area under the peak remains constant) and the peak shape changes, sometimes in a quite complicated fashion (e.g. experiment D2). The perturbation of the doping distribution introduced by the analysis technique cannot, in such cases, adequately be described by any number of interface widths and to report but one is to throw away most of the information on that interaction. The shape of the broadened marker, however, contains all the information. We tried to understand the trends in peak shapes described above.

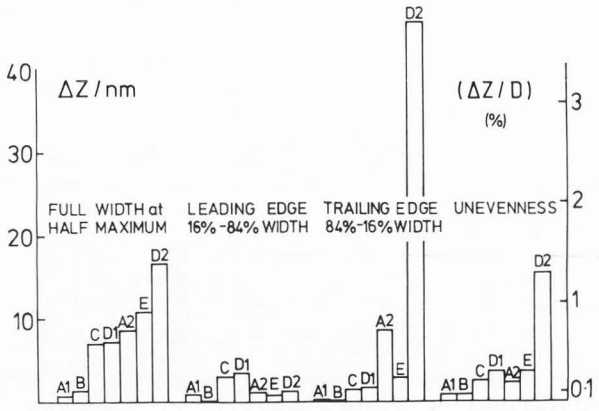

Figure 4

Bar charts representing the change in peak interface widths between peak 3 and peak 26/28 (average of two) in the seven depth profiles, a depth increment D of 1200nm. Both the absolute change in depth resolution Δz, and the change as a percentage of the depth increment, $(\Delta z/D).100$ are shown.

We already knew that uneven etching was responsible in large part for the loss of depth resolution with depth in experiment D1, (McPhail et al 1986). We had monitored the breakthrough to buried dopant layers as the depth profile proceeded using a technique called secondary ion imaging. The deflection voltages driving the raster scanner plates are simultaneously used to drive the x and y plates of a variable persistence storage oscilloscope and the intensity of the secondary ion signal used to modulate the brightness of the image on the cathode ray screen. A series of boron images were taken as the crater passed through a buried boron rich layer (Figure 5). The breakthrough occurred in four lobes first and the centre of the crater last, suggesting that the base of the crater was not flat, the lobes representing the deepest points. Talystep scans on the final etch pit confirmed the suspected topography and by making measurements in four scan directions a contour map was produced (Figure 6). The maximum unevenness in the gated area (175μm x 175μm) of the crater was 20nm, which is approximately 1.2% of the total depth (1.67μm). Thus secondary ion imaging is a sensitive diagnostic technique, more accurate indeed than surface profilometry. Chemical imaging of the breakthrough pattern in experiment D2, on the same instrument but on a different day after retuning, again revealed a non-uniform breakthrough pattern, but one completely dissimilar to that in D1. Figure 7 shows successive images as the crater passed through peak 8. The bottom half of the crater reached the boron-rich layer first and there was then a slower breakthrough by the rest of the crater, the boron secondary ions appearing as a bright bar that moved parallel to the x-axis. Careful measurements were made on the etch pit from this experiment at high magnifications (Figure 8) and they revealed a gross unevenness in

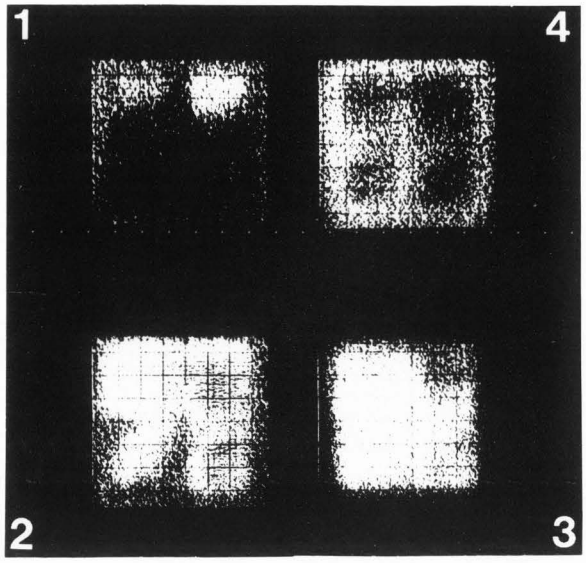

Figure 5

Boron channel secondary ion images at four successive intervals in the depth profile showing the breakthrough pattern to a buried boron-rich layer in experiment D1. The boron secondary ions (bright field) appear in four lobes first, suggesting these are the deepest points, and the centre of the crater last. Image field 400μmx400μm

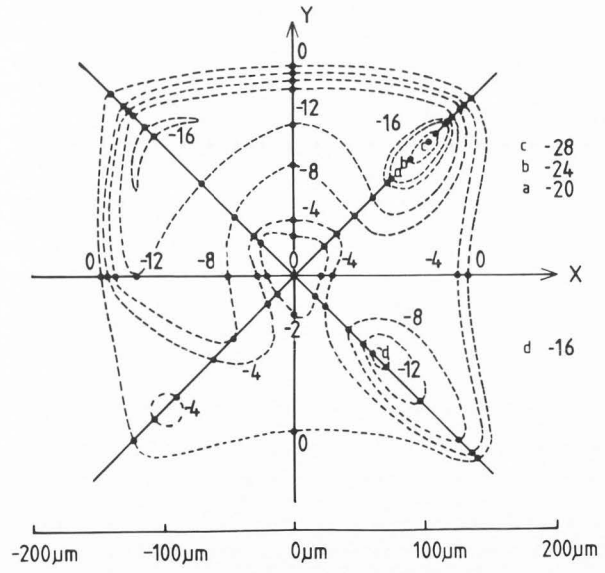

Figure 6

A contour map of the crater base of experiment D1, built up from four talystep scans. The dots are measured points of depression in nanometres relative to the centre of the crater. The agreement with the images in Figure 5 is good.

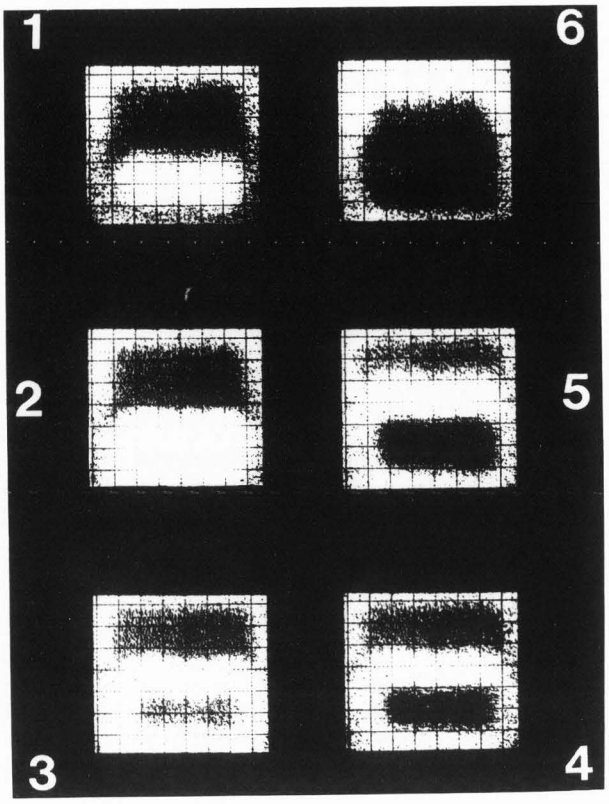

Figure 7

Six successive boron channel secondary ion images in experiment D2 illustrating the breakthrough pattern as layer 8 (0.348μm) is traversed.

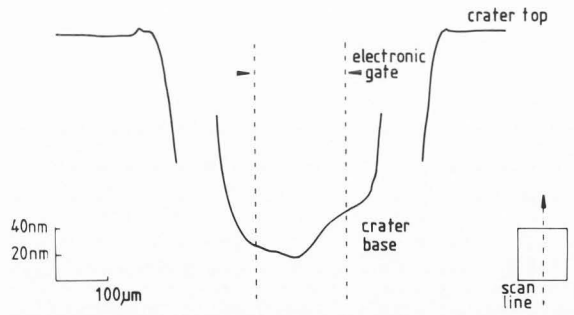

Figure 8

A crater depth measurement, at high magnification on the crater from experiment D2. The 'Y' scan direction is shown.

the y-scan direction, the base consisting of a flat half and a bevelled section. The x-scan direction was flat, which emphasises the importance of making measurements in both scan directions. The problem has now been traced to the raster scanner and has been corrected. The unevenness in the crater bases in experiments D1 and D2 was sufficient to explain the observed peak broadening as those experiments progressed. We now measured the craters in the other experiments to see if the same explanation was valid in those cases.

Whilst it is difficult to measure absolute crater depths to better than a few percent using a Dektak or Talystep, one can resolve the topography of the base to an accuracy of 2nm or less. To do so one progressively increases the magnification whilst making adjustments to ensure that the surface level remains flat. The base of the crater will go 'off-range'. When the top of the crater appears flat at high magnification (e.g. 500,000) the stylus pressure is increased and the base of the crater traversed. The average unevenness of the craters (defined as the average of the absolute differences from the mean depth) from the seven experiments is plotted in Figure 4 and there is a clear correlation between this parameter and the loss of depth resolution with depth Δz (full-width at half-maximum). It would appear that uneven etching was the dominant mechanism for peak broadening in all these experiments. It was not yet clear why the broadening sometimes affected the leading edge most and sometimes the trailing edge most and so a model of the etching process was developed.

Modelling the effects of uneven etching

The uneven etching model (McPhail et al 1987) simulates depth profiling through a known, laterally homogeneous, dopant distribution p(z), in which the unevenness in the crater base is a fixed fraction of the total average depth D, Figure 9. This is the physical situation that is obtained if the uneven etching arises from a non-uniform primary beam flux across the surface (Werner 1982). The unevenness function f(x,y) is derived from depth measurements on the crater base in several scan directions and is defined as:

$$f(x,y) = d(x,y)/D \qquad (3)$$

where f(x,y) is an array of numbers usually close to unity. The calculations are performed using a program written on a VAX 11/750. The program requires f(x,y) and p(z) as input parameters. The SIMS depth profile is allowed to proceed in a series of equal depth iterations (i=1 to N). The observed SIMS signal is proportional to the number of dopant atoms removed per depth iteration. The calculation takes into account the different depths and different volumes of the volume elements due to the uneven erosion rate across the surface yielding an expression for the SIMS signal per iteration,

$$C(n) = aT \sum_x \sum_y (D/N)\, f(x,y)p(z)\, dxdy \qquad (4)$$

where a is the ionisation probability and T the instrumental transmission. This model predicts, for example, that a ten percent unevenness will

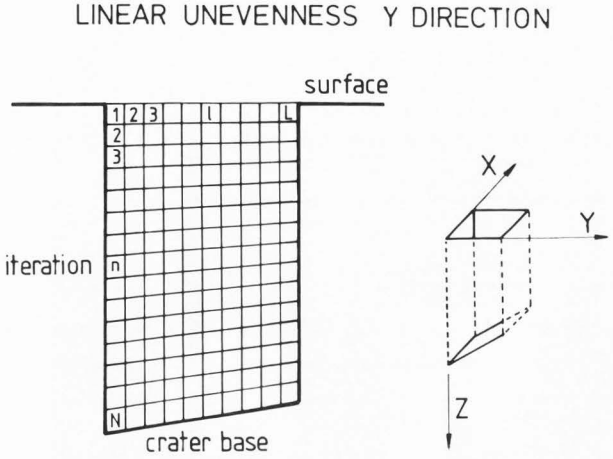

Figure 9.

Basis of the simulation routine for uneven etching showing the special case of unevenness in one direction only (the y direction). Notice that in the n'th iteration the centres of the volume elements are at different depths and that the volume elements on the left are slightly larger than those on the right.

broaden a gaussian implant, on the trailing edge by less than three percent but will limit the number of periods of a periodic dopant distribution that may be resolved to ten.

We used the shape of peak 3 in experiment D1 as the doping distribution. This is close to the surface (100nm) and as such represents a marker broadened only by beam induced broadening effects ($B.z \sim 0.6$nm). This marker was placed at depths below the surface corresponding to the depths of reference peaks (3, 5, 8, 10, 12, 26, 28) and the program then used to simulate the effect of an uneven crater passing through it. The unevenness functions used were derived from craters D1 and D2 (see Figures 6 and 8). The results of the simulation programs for experiments D1 and D2 are shown in Figures 10 (a, b, c) and Figures 11 (a, b, c,). There is good agreement both qualitatively and quantitatively. The modelling successfully predicts that in experiment D1 most of the broadening will be in the leading edge, whereas in D2 all the broadening will be in the trailing edge. The calculated leading edge for D1 (Figure 10b) departs from the experimental value at large depths, due to the predicted shoulder in peak 28 which is not observed experimentally. This probably reflects the difficulty of measuring the unevenness in the crater base. One should also note that very small voids ($\sim$10μm) cannot be detected by stylus tracking methods and this can have serious implications, for example when depth profiling for aluminium in silicon-on-sapphire (Dowsett et al 1986).

The observed trends in depth resolution-depth curves can also be understood qualitatively by considering the rate of removal of material per iteration as the crater base passes through an abrupt marker layer. If the unevenness is a linear

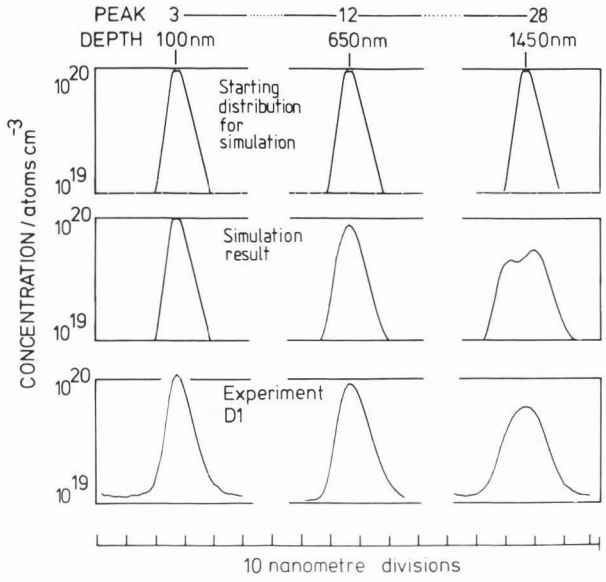

Figure 10a

The result of the modelling for experiment D1. Only three peaks are shown, highly magnified. P(z) consists of three peaks at depths of 100nm, 650nm and 1450nm. The unevenness function was derived from the crater depth measurements shown in Figure 6.

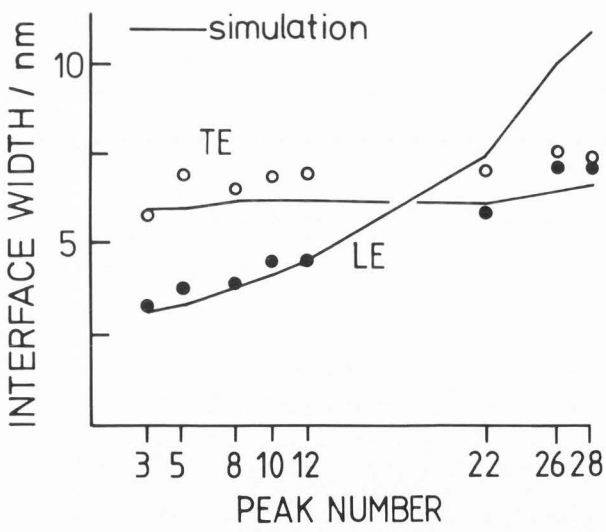

Figure 10b.

A comparison of the experimental interface widths and those produced by the simulation modelling program in experiment D1. The leading and trailing edge interface widths are shown here. Circles are experimental values, solid lines modelling results.

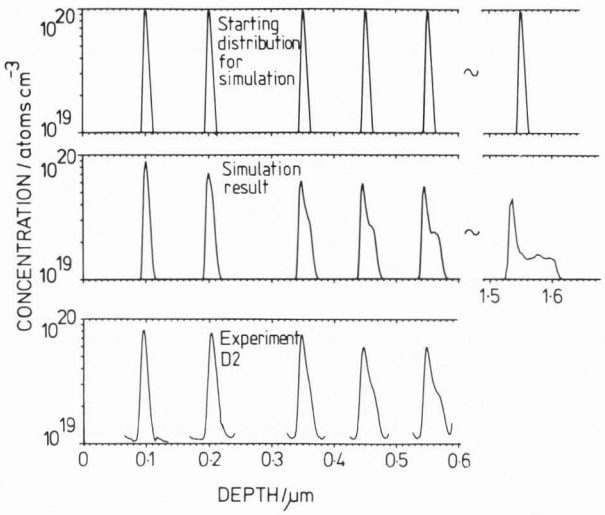

Figure 11a

The result of the modelling for experiment D2. Experimental peaks 3,5,8,10 and 12 are shown compared to the results of modelling. The unevenness function was derived from the crater depth measurement shown in Figure 8. The experiment was terminated at peak 16 but we also show the theoretically predicted shape that peak 31 would have had with that crater topography.

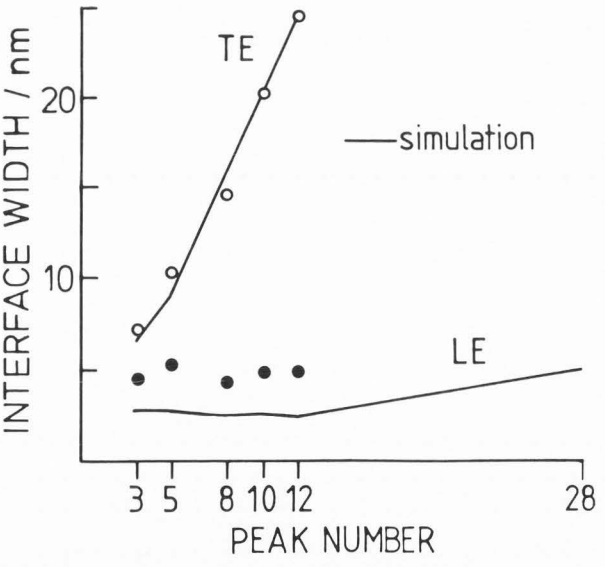

Figure 11b

A comparison of the experimental interface widths and those produced by the simulation modelling program in experiment D2. The leading and trailing edge interface widths are shown here. Circles are experimental values, solid lines modelling results.

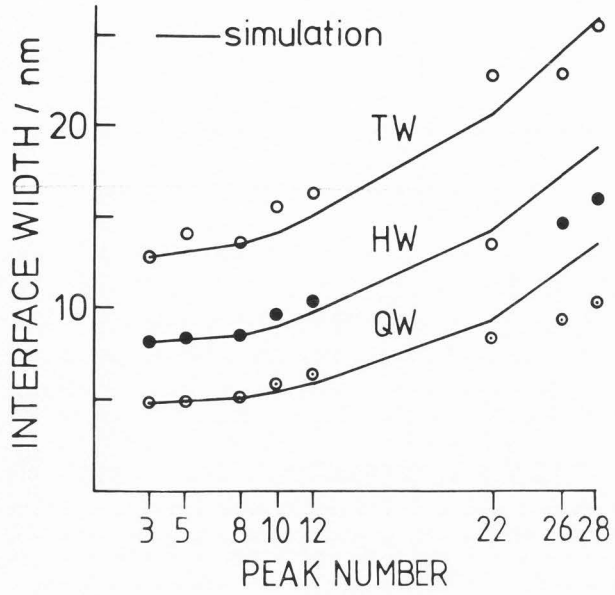

Figure 10c

Comparison of the experimental peak widths with those produced by the simulation routine in experiment D1 / simulation D1.

function of x and y, (as in C) or the crater base is convex, that is the deepest parts of the crater have the steepest slope (dx/dz, dy/dz), then most of the broadening will be in the (steeper) leading edge (as in D1). If the crater base is sufficiently concave, however, that is if the deepest parts of the crater have the shallowest slope (dx/dz, dy/dz), then broadening will occur mainly in the trailing edge (as observed in A2, D2 and E).

The result D2 is particularly interesting as the crater base consists of a deep flat section and an approximately linear bevelled section (which together form a 'concave' topography). The profile can be regarded as a series of independent profiles proceeding at different rates in which the depth scales are then forced equal. As the profile proceeds the flat section continues to generate a 'true' profile to which are added an infinite series of contributions from the bevelled section. Since these points lag behind the flat section their contributions are stretched during the depth calibration, leading to the tail on the deep part of the peak. As the absolute unevenness on the bevel increases with depth the tail is broadened and interferes less with the 'true' signal thus tightening that feature and appearing to reduce the HW width. The simulation routine predicts that the peak height approaches an asymptote and the leading edge remains constant in time. The experiment seems to confirm this. Unfortunately this prediction cannot be further tested experimentally as the broadening tail begins to interfere with the leading edge of the next peak.

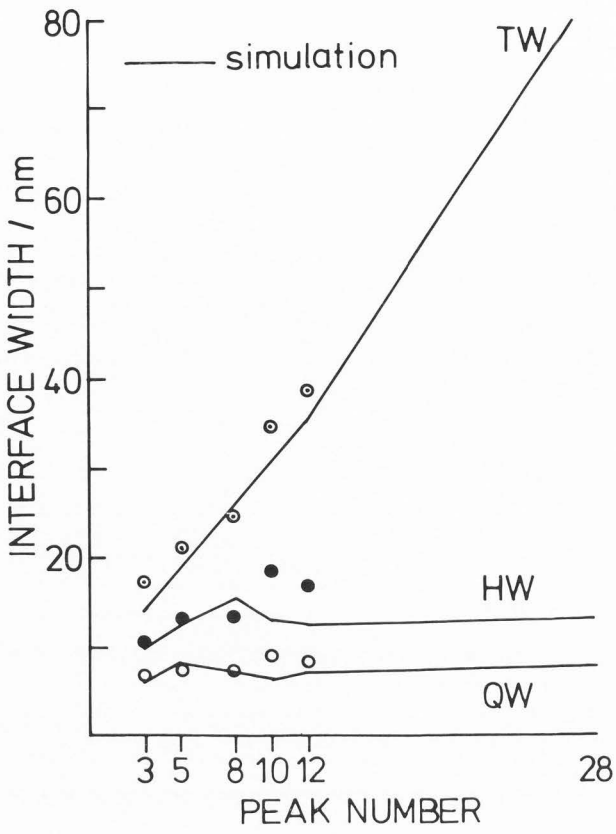

Figure 11c

Comparison of the experimental peak widths with those produced by the simulation routine in experiment D2 / simulation D2.

Variation in peak shapes with beam energy

Intercomparison of the peaks in experiments A1 and B, where there was no significant loss of depth resolution (peak broadening) with depth, reveal that the peaks in experiment B are significantly broader than those in experiment A1. The average peak widths in these two experiments are given in Table 2 (both Camecas).

Table 2

The peak widths observed in experiments A1 and B Average of values from peaks 3,5,8,10,12,26 and 28 are shown with standard deviations in brackets. See Figure 3 for interface width definitions.

	LE/nm	TE/nm	LU/nm	LD/nm
Exp. A1	4.3 (1)	6.3 (0.4)	2.8 (0.3)	4.9 (0.2)
Exp. B	3.9 (1)	7.7 (0.3)	2.9 (0.7)	6.0 (0.4)

	TW/nm	HW/nm	QW/nm
Exp. A1	6.0 (0.6)	9.30 (0.8)	14.6 (2)
Exp. B	6.4 (0.5)	10.1 (0.6)	16.5 (0.7)

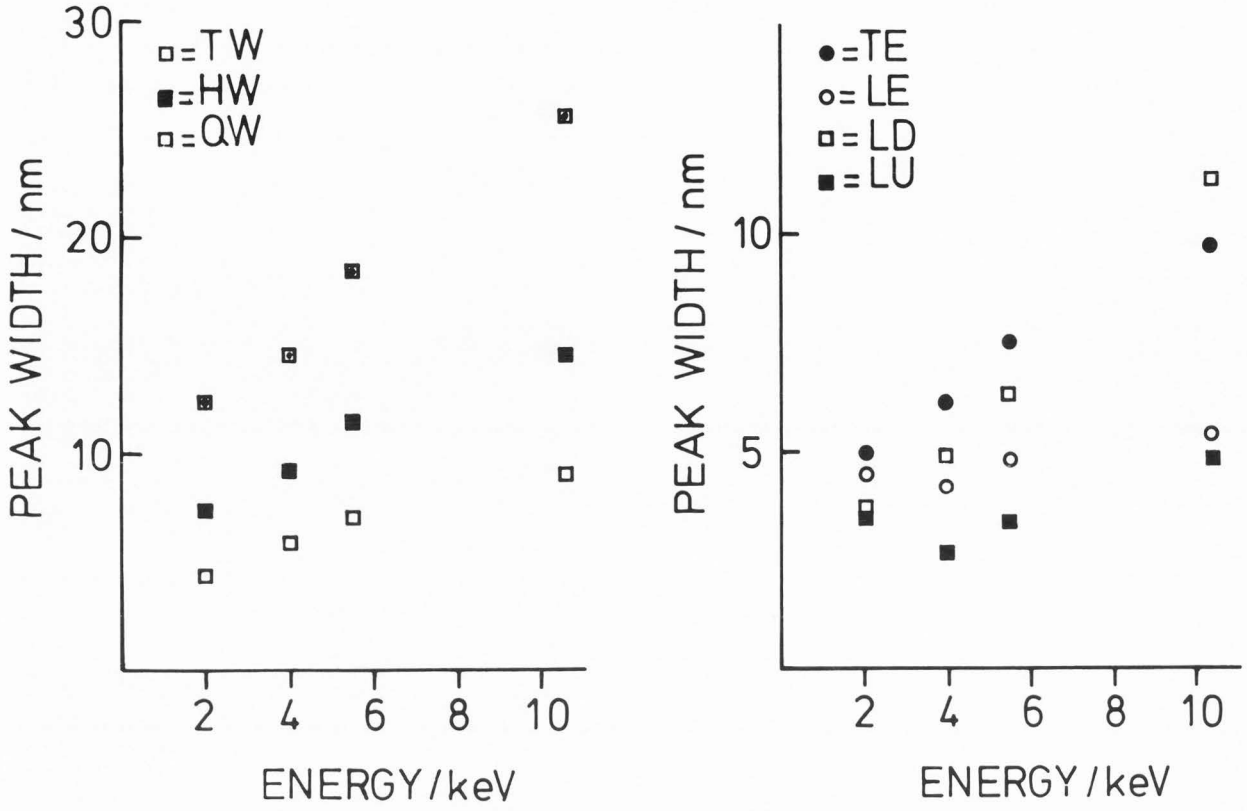

Figure 12 The interface widths of peak three as a function of the primary beam energy.

The most significant difference is in the widths of the trailing edges (TE and LD). These widths represent the true widths of the peaks together with a contribution from beam induced broadening effects. The differences in average peak widths between experiments A1 and D of 0.8nm in the half widths (HW), of 1.4nm in the trailing edge interface widths (TE) and of 1.1nm in LD, the decay length , reflect the different primary beam energies used (4 and 5.5 keV). It follows that by profiling the sample at several beam energies one may be able to estimate the true layer widths by extrapolation of their apparent widths to zero energy. A series of profiles was completed on instrument A at primary beam energies of 10.5keV, 5.5keV, 4.0keV and 2.0keV to deduce the 'true' width of peak 3. The relationship between the peak interface widths and beam energy is shown in Figure 12. Unfortunately there are large error bars (10%) on the widths because the analyst used insufficient data density (see Table 1). This makes accurate measurements difficult. (The interface widths were measured by quadratic interpolation between the data). The apparent layer width of peak 3 at 'zero primary beam energy' (by linear extrapolation) is less than 6.5nm ± 1nm wide (HW). The effect of reducing the probe energy is to remove the peak asymmetry. The 'true' interface widths are less than 5nm (LE,TE) and the 'true' decay lengths less than 3nm (LU) and 4nm (LD), respectively.

The lowest energy used, 2.0keV, is close to the operational limit for the Cameca due to the parabolic trajectories that low energy primary ions undergo near the sample surface as they experience the high secondary ion extraction field. Indeed at this energy the crater was of poor shape and a rapid loss of depth resolution with depth reported. This problem partially offsets the advantages of optical gating and high transmission. Furthermore one cannot decouple the energy and angle of incidence in the Cameca, in order to determine their effects independently, a serious shortcoming from which the Atomika does not suffer. One possible solution would be to add a neutral primary beam facility to the Cameca. Degreve and Lang (1985) have used such a modification to overcome charging of badly insulating samples. Unfortunately, the neutral beam was static and produced an extremely curved crater, quite unsuitable for high depth resolution studies. One possible solution, they suggested, was to mechanically raster the sample. Alternatively the ions could be rastered before entering the neutralisation chamber. It is not yet clear whether neutral beams of sufficient intensity, purity and uniform flux density will be developed for depth profiling work and it is to be hoped that manufacturers such as Cameca can be encouraged to undertake such development work. Indeed a fast atom source is included on the new VG IX70S.

A possible alternative to depth profiling

Since the fundamental mixing processes can never be removed entirely from SIMS depth profiling and work at low energy is both difficult and subject to error, alternative methods of resolving thin layers are being considered. One method, suggested by the very poor crater shape observed in experiment D2, is to deliberately bevel the samples using ion beam lithography. It may thus be possible to magnify layers thinner than the depth resolution of the technique (in the depth profiling mode) into surface stripes wider than the lateral resolution of the technique (in the imaging mode). The bright bars in Figure 7 are approximately 85μm wide (total area imaged is 400μm x 400μm), thus the bevel geometry in the bottom of the crater at that depth in the profile (0.348μm), 12.5 nm deep x 150μm across, implies a layer thickness of 7nm. This is in good agreement with the low energy value quoted above. The resolution of the layer is hindered by the coarse beam size used (50μm HW) and it is important, therefore, when bevelling and imaging to magnify the layer into a surface stripe much wider than the imaging probe diameter. We can now produce bevel magnifications on EVA 2000 in the range 10^4 to 10^5 using our raster scanner in the line-scan mode and applying a ramp to the other plate of increasing dwell time. In Figure 13 we show the results of imaging the test sample after six such bevels. At low magnifications there are several bars in the field of view. The apparent width of these bars is mainly due to the finite beam width (20μm). As the magnification is increased, however, the number of layers in the field of view decrease and their width increases. Finally there is only one layer (corresponding to peak 2, 50nm below the surface) the width of which increases with bevel magnification. The apparent layer thickness T from bevel 1 is the apparent layer width on the bevel W, divided by the magnification M. In this case the stripe was 37.5μm wide, the magnification 2330 and thus the deduced layer thickness T was 16nm. In all other cases T was 9.5nm ± 1nm (up to a magnification in 6 of 41700). We can deduce, therefore, that a bevel magnification of at least 10,000 is required for these layers with such a coarse imaging probe. Note that in the cases where more than one layer is imaged one can also estimate the widths directly, given that the spacing between layers is 50nm.

There are several other problems with such an approach, not least the fact that the ion beam lithography itself introduces damage and mixing into the surface region of the sample. In this example boron atoms from the buried layer will be mixed both upwards and downwards. This mixing will be magnified in the same ratio as the layer itself. The technique will have no advantage over depth profiling unless this mixing can be removed. One possibility is chemical etching. In silicon the mixing region corresponds to a region oxidised by the oxygen primary ion beam and can be removed with an etch such as hydrofluoric acid. Approximately 22.5 nm of oxide is removed in this way, a figure that closely agrees with scanning electron microscopy data on the oxidized surface (Augustus et al, 1987). Secondary ion imaging of such layers using a sub-micron probe, having first removed the damaged surface region with a chemical etch, will, in principle, give very accurate layer width measurements (McPhail and Dowsett, 1987). The imaging probe will itself re-mix the surface somewhat and we are trying to model this effect at present. Another interesting feature of the bevel-etch-image technique is that after chemical etching the silicon grows a native oxide layer a nanometre or more thick. This leads to secondary ion yield enhancement during acquisition of the first few images . One limitation to the sensitivity of the technique, however, is that only a small depth of material may be consumed during the acquisition of an image to avoid lateral movement of that image.

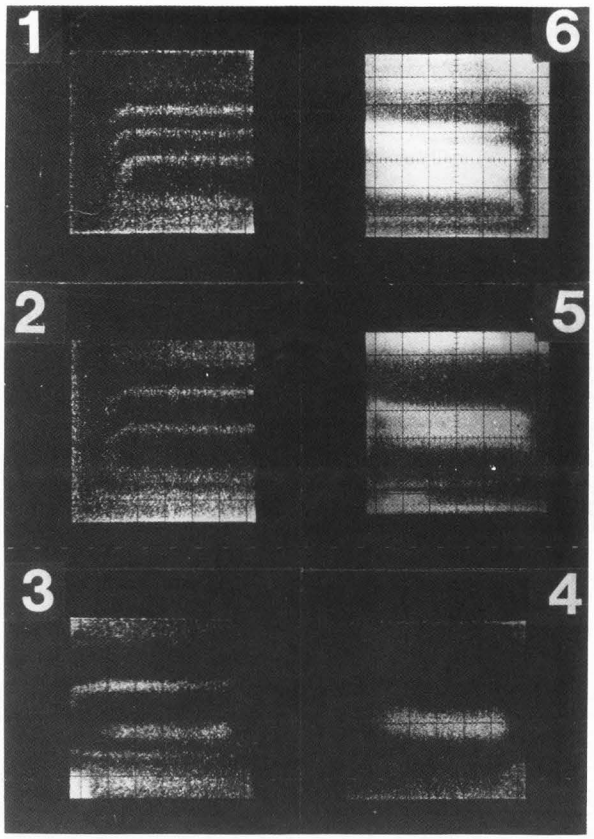

Figure 13

Chemical images of the test structure, produced by bevelling the sample at various angles using ion beam lithography, and then imaging the bevelled area with a well focussed oxygen ion beam (~20μm). As the bevel magnification is decreased the number of layers in the field of view (1000μmx1000μm) increases.

Image 1	W=37.5μm	M=2330	T(apparent)=16.1nm
Image 2	W=37.5μm	M=3640	T(apparent)=10.3nm
Image 3	W=50μm	M=5000	T(apparent)=10.0nm
Image 4	W=113μm	M=13540	T(apparent)= 8.4nm
Image 5	W=212μm	M=23800	T(apparent)= 8.9nm
Image 6	W=425μm	M=41700	T(apparent)=10.2nm

Conclusions

We have investigated the depth-resolution depth characteristics of five Secondary Ion Mass Spectrometry instruments of three different ion-optical configurations using a boron-in-silicon modulated dopant structure grown by silicon MBE. The near surface peaks appeared narrow and asymmetric in all seven experiments, being broadened by fundamental processes such as atomic mixing and recoil implantation. The extent of this broadening could be reduced by lowering the primary beam energy. Further peak broadening occurred as the profile proceeded in all cases but two. It varied both in extent and in form from one experiment to another, in some cases mainly affecting the leading edge, in other cases the trailing edge of the peaks. Thus the 'order of merit' of the experiments depended upon the definition of depth resolution (LE, TE, HW) used for comparison and it follows that it is incorrect to assess the depth resolution of a SIMS instrument on the basis of a single interface width. The loss of resolution with sputter depth was due to uneven etching and an uneven etching model explained the extent and the form of the peak broadening quantitatively. Uneven etching indicates a non-uniform primary beam current density across the crater surface due to problems with the primary beam optics. An unevenness of the order of one percent is the rule and a perfectly flat crater base the exception in SIMS depth profiling.

For high depth resolution work both the instrumental and fundamental broadening processes must be minimised. Loss of depth resolution with depth can be minimised on instruments such as the Cameca which employ optical gating and a high secondary ion transmission. This allows collection of ions from a very small area at the centre of the crater ($< 50\mu m^2$ compared to $> 400\mu m^2$ in the Atomika). However, unlike the Atomika and EVA 2000, the Cameca cannot be operated at the very low primary beam energies (<2keV) required to minimise the fundamental broadening processes nor can the primary beam energy and angle of incidence be de-coupled. An instrument that combined a scanned neutral primary beam with optical gating and high secondary ion transmission would seem appropriate to high depth resolution work.

Bevelling etching and imaging may be a viable alternative to the depth profiling of thin layer structures.

References

Augustus PD, Spiller GDT, Dowsett MG (1987) Cross-sectional transmission electron microscopy studies of primary beam damage at the bottom of SIMS craters eroded in silicon. Proceedings of SIMS VI, Versailles, 1987. John Wiley, in press.

Degreve F, Lang JM (1985) Use of a fast atom beam in ion microscopy (FABIM) for the analysis of poorly conducting materials. Surface and Interface Analysis, 7(4), 177-187.

Dowsett MG, Parker EHC (1983) Experimental study of electrode materials for use in a cold-cathode oxygen discharge. Int. J. Mass Spectrometry Ion Physics, 52, 299-309.

Dowsett MG, Parker EHC, McPhail DS (1986) High dynamic range depth profiles for aluminium in silicon-on-sapphire. Proceedings of SIMS V, Washington 1985, 340-342. Springer-Verlag.

Gavrilovic J (1986) Depth resolution in profiling of thin GaAs-GaAlAs layers. Proceedings of SIMS V, Washington 1985, 360-362. Springer-Verlag.

Gruen DM, Pellin MJ, Young CE, Calaway WF (1987) The impact of high efficiency laser post-ionisation techniques on surface and bulk mass spectrometric analysis. Proceedings of SIMS VI, Versailles 1987. John Wiley, in press.

Honig RE (1986) The growth of Secondary Ion Mass Spectrometry (SIMS): A personal view of its development. Proceedings of SIMS V, Washington 1985, 2-15. Springer-Verlag.

King BV, Tsong IST (1985) Deconvolution of atomic mixing effects from SIMS depth profiles. Nucl. Insts. and Methods in Physics, B7/8, 793-797.

Kubiak RAA, Leong WY, Parker EHC (1985) Enhanced sticking coefficients and improved profile control using boron and antimony as co-evaporated dopants in silicon MBE. J. Vac. Sci. and Technol., B3(2), 592-595.

Levi-Setti R, Crow G, Wang YL (1985) Progress in high resolution scanning ion microscopy and secondary ion mass spectrometry imaging micro-analysis. Scanning Electron Microsc. 1985; II: 535-551.

Magee CW, Harrington WL, Honig RE (1978) Secondary ion quadrupole mass spectrometer for depth profiling-design and performance evaluation. Rev. Sci. Instrum., 49, 477.

Magee CW, Honig RE, Evans CA (1982) Depth profiling by SIMS-depth resolution, dynamic range and sensitivity. Proceedings of SIMS III, Budapest, 1981, 172-185. Springer-Verlag

McPhail DS, Dowsett MG, Parker EHC (1986) Loss of depth resolution with depth in Secondary Ion Mass Spectrometry (SIMS) due to variations in ion dose density across the rastered area. Vacuum, 36 11/12, 997-1000.

McPhail DS, Dowsett MG, Houghton R, Fox H, Leong WY, Patel GK, Parker EHC (1987) Quantifying the effects of uneven etching during the SIMS analysis of periodic doping structures grown by silicon MBE. Surface and Interface Analysis, in press.

McPhail DS, Dowsett MG (1987) Bevelling-Etching-Imaging: a novel technique for resolving thin layer structures. Proceedings of SIMS VI, Versailles, 1987. John Wiley, in press.

Werner HW (1982) The depth dependence of the depth resolution in sputter profiling. Surface and Interface Analysis, 4(1), 35-40.

Williams P (1985) Limits of quantitative microanalysis using secondary ion mass spectrometry. Scanning Electron Microsc. 1985; II: 553-561.

Wittmaack K, Wach W (1981) Profile distortions and atomic mixing in SIMS analysis using oxygen primary ion beams. Nucl. Insts. and Methods, 191, 327-334.

Discussion with Reviewers

J.D. Brown: Reference is made in the text to the apparent depths at which peak 31 appears in the profile. Further, the craters A1 and D1 were remeasured on the same Talystep and the differences confirmed. No mechanism exists whereby the position of the peaks can be shifted by sputtering artifacts. Would the authors comment on the possibility of variations in layer thickness of the sample from specimen to specimen or sputtering by a neutral beam component leading to these differences ?

Authors: Silicon epilayers can vary in thickness along a wafer diameter by several percent, as mentioned in the experimental section, and since specimens were taken at random from the grown wafer, this is sufficient to produce the observed effect. There are, incidentally, sputtering artifacts which can shift peak positions. Uneven etching is one example. Refer to the simulation result in Figure 11a. The model predicts that the maximum of peak 31 is shifted towards the surface relative to the starting distribution. A second and perhaps more serious perturbation will occur if the primary beam current varies during the analysis. I believe that the difference in epilayer thickness is a 'true' result. Thus one might be justified in presenting the depth profiles with the substrates (and not the surfaces) aligned.

R. Levi-Setti: For each experiment the depth increment (dz) between boron data points is > 1.5nm, yet you claim many changes in width are less than dz (Figure 4). Even with averaging, width resolution cannot be better than dz, nor can Δz. Recourse to interpolation arguments is not compelling.

Authors: We take this point. The bars on the bar chart should perhaps have error bars of about 1nm on them. The analyst has a considerable problem in choosing the sputtering conditions for this sample. He requires a high data density for accurate peak resolution and a reasonably quick analysis time, to minimise instrumental drift. Suppose two mass channels, boron and silicon, are run. If the depth increment between boron data is 1nm and the time increment 2s then the analysis will take about 3600s (to 1.8μm) and will generate 3600 data. Clearly 0.1nm resolution will require much shorter counting times (not possible on the Cameca due to hysteresis effects) or a longer analysis time and in both cases will generate more data than many computer data systems can cope with.

R. Levi-Setti: In McPhail et al, (1987) you deduce a FW of 1.4 $\pm$ 1nm for the boron spikes in this sample, much less than the values given in this paper. Have you re-evaluated your thinking?

Authors: The apparent average peak width in that experiment was 7.5nm. We then deducted the width of a boron marker marker layer broadened under the same analysis conditions (6.1 nm) to deduce a 'true width' for the experimental peak of 1.4nm. This is clearly not a valid procedure for layers similar to or thinner than the mixing range of the primary beam and deconvolution software that is being developed at present. The methods presented here, extrapolation of the peak width to zero primary beam energy and bevelling-etching-imaging, are considered more reliable.

J.A. Kilner: In figure 13 several chemical images of the bevelled sample are shown. In images (1) and (2) clear horizontal bars show the presence of doped layers. These are well separated on the RHS of the image but become curved and distorted at the LHS of the image. What is the explanation for this distortion?

Authors: The imaged area is not quite centered with respect to the bevelled area and on the left hand side we are imaging the side wall of the bevel. The layers 'turn' towards the deep end of the bevel, when viewed from above.

Acknowledgements

Thanks are conveyed to the organisers of SEM for supporting my visit to the SEM conference in Hamilton, Ontario in 1987. Acknowledgement is made to the silicon MBE team and technical staff at Warwick University, and to the SIMS operators at Loughborough Consultants, Surface Analysis Technology, Philips and British Telecom. Acknowledgement is also made to to the Director of Research and Technology of British Telecom for permission to publish this paper. The paper is dedicated to M.M.Faktor, former Professor of Chemistry at Queen Mary College.